Large-eddy simulation of flow over barchan dunes

M. Omidyeganeh [(1)], U. Piomelli [(1)], K. T. Christensen [(2)], and J. L. Best [(2)]

1. Queen's University, Kingston, CA – omidyeganeh@me.queensu.ca, ugo@me.queensu.ca
2. University of Illinois, Urbana-Champaign, USA – ktc@illinois.edu, jimbest@illinois.edu

Abstract

We have performed large-eddy simulations of turbulent flow over barchan dunes in a channel with 5 differing interdune spacings in the downstream direction at moderate Reynolds number, Re_∞=25,160 (based on the free stream velocity and channel height). Simulations are validated against experimental data (at Re_∞=59,000); the largest interdune spacing (2.38λ, where λ is the length of the barchan model) presents similar characteristics as the isolated dune in the experiment, indicating that at this distance the sheltering effect of the upstream dune is very weak. We provide 3D realizations of the mean and instantaneous flow that allows us to explain some features of the flow relevant to sediment transport. Barchan dunes induce two counter-rotating streamwise vortices, along each of the horns, which direct high-momentum fluid toward the centerline symmetry plane and low-momentum fluid near the bed away from the centerline. Distribution of the bed shear stress, characteristics of the separation and reattachment regions, and instantaneous wall turbulence are discussed. The interdune spacing significantly alters the turbulent flow over the stoss side of the dunes. The characteristics of the separated-shear layer are altered quantitatively; the separation bubble is smaller, the separated-shear layer is stronger, and the bed shear stress is larger at smaller interdune spacings.

1. INTRODUCTION

The interaction of turbulent flow fields with a mobile sand bed, when the flow is unidirectional and sand supply is limited, results in the formation of barchan dunes in aeolian and fluvial environments. Barchans have a crescentic topography with horns elongated in the downstream direction (Kroy *et al.* 2005), and are extensively observed in deserts on Earth (Bagnold 1941; Lancaster 1995) and on Mars (Breed *et al.* 1979), but only rarely in rivers and oceans (McCullogh *et al.* 1964; Allen 1968). The linear relationship between the width of the dune, its height and length and its three-dimensional shape are well understood (Bagnold 1941; Hesp *et al.* 1998). Barchans rarely exist as isolated forms and may occur in large fields (Hersen *et al.* 2004) of a few hundred square kilometers in area (Lettau *et al.* 1969). Their significant effects on the flow field and sediment transport have attracted researchers to study fluid and morphological dynamics in environments with barchans.

Most of the measurements and calculations of flow and sediment transport have been performed on the streamwise-wall-normal symmetry plane of barchans, over the windward stoss side (Lancaster 1985; Lancaster *et al.* 1996; Wiggs *et al.* 1996; McKenna *et al.* 2000; and Palmer *et al.* 2011). Theoretical efforts have also usually considered transverse dunes (Lancaster 1985; Frank *et al.* 1996; Lancaster *et al.* 1996; Wiggs *et al.* 1996; McKenna *et al.* 2000) and assumed the law-of-the-wall to be valid, although velocity profiles often do not obey the logarithmic law of the wall over barchan dunes (Frank *et al.* 1996; Wiggs *et al.* 1996; McKenna *et al.* 2000). Although transverse dunes share some mean-flow features with barchan dunes, such as the separation of the flow at the crest, the separated-shear layer over the lee side and the developing internal boundary layer, the three-dimensional mean flow around barchans introduces additional complexities that affect the turbulence.

A few numerical studies have been conducted of flow over three-dimensional barchan dunes (Wippermann *et al.* 1985; Takahashi *et al.* 1998); they generally suffer from a low grid resolution and inaccurate models. Reynolds-averaged Navier-Stokes solvers in 2D (Parsons *et al.* 2004) and 3D (Hermann *et al.* 2005) provide mean-flow characteristics (flow acceleration/deceleration, separation, reattachment, and reversal) with qualitative agreement with the literature, but do not provide

information on the instantaneous flow structures observed in experiments (McKenna *et al.* 2000; Franklin *et al.* 2011) and their importance; for instance, elongated sand streaks observed on the stoss side of dunes represent significant contribution of wall turbulence to sediment transport (Franklin *et al.* 2011; Charru *et al.* 2012).

The effects of interdune-spacing on dune dynamics have been largely ignored, despite the fact that the spacing affects the flow on the lee side of the upstream dune and the stoss side of the downstream dune (Fernandez et al., 2006), and may change the mechanisms of sediment transport (Walker *et al.* 2003; Baddock *et al.* 2007; Palmer *et al.* 2011). The importance of secondary flows in the lee side on intermittent sediment transport over the stoss side of the downstream dune was studied by Walker *et al.* (2003); high shear-stress variability at the reattachment zone inhibits sediment deposition and can cause deformation of the stoss side of the downstream dune. At interdune spacings close to the separation-bubble size, regular deformation models (McLean *et al.* 1986) cannot explain the flow physics, even for transverse dunes (Baddock *et al.* 2007). Palmer *et al.* (2011) conducted a series of novel experiments on the effects of interdune spacing on the features of the separated shear-layer, separation bubble size and approaching turbulence structures on the downstream dune stoss side over the centerline symmetry plane. The sheltering effect of the upstream dune on the flow over the downstream dune was identified, in which the separated vortices are advected downstream and transported energy to smaller scales.

However, all efforts so far lack an accurate representation of the bed shear-stress, which provides insight on the sediment transport mechanisms in a three-dimensional view. Turbulent flow over the lee side of the dune, where the flow separates at the crest and broad ranges of length- and time-scales are introduced into the turbulence spectrum, is poorly understood. The three-dimensional mean flow and turbulence characteristics have yet to be studied with reasonable resolution. The significant contribution of the interdune spacing on the mean-flow and instantaneous flow features has also to be examined in detail. Herein, we aim to perform a series of resolved large-eddy simulations of flow over a model barchan dune (Palmer *et al.* 2011) at various interdune spacings, in order to obtain a more comprehensive 3D understanding of mean flow characteristics and turbulence coherent structures.

2. PROBLEM FORMULATION

In large-eddy simulations, the velocity field is separated into a resolved (large-scale) and a subgrid (small-scale) field, by a spatial filtering operation (Leonard 1974). The non-dimensionalized continuity and Navier-Stokes equations for the resolved velocity field are

$$\frac{\partial \overline{u_i}}{\partial x_i} = 0, \tag{1}$$

$$\frac{\partial \overline{u_i}}{\partial t} + \frac{\partial \overline{u_i}\,\overline{u_j}}{\partial x_j} = -\frac{\partial \overline{p}}{\partial x_i} - \frac{\partial \tau_{ij}}{\partial x_j} + \frac{1}{\mathrm{Re}_\infty}\frac{\partial^2 \overline{u_i}}{\partial x_j \partial x_j}, \tag{2}$$

where $Re_\infty = U_\infty h/\nu$, h is the channel height, and U_∞ is the free-stream velocity of an equivalent open channel flow simulation without surface roughness (dune). x_1, x_2, and x_3 are the streamwise, vertical and spanwise directions, also referred to as x, y and z. The velocity components in these directions are, respectively, u_1, u_2 and u_3 (or u, v and w). An overline denotes a filtered quantity, and $\tau_{ij} = \overline{u_i u_j} - \overline{u_i}\,\overline{u_j}$ are the subgrid stresses, which were modeled using an eddy-viscosity assumption

$$\tau_{ij} - \delta_{ij}\tau_{kk}/3 = -2\nu_T \overline{S_{ij}} = -2C\overline{\Delta}^2 |\overline{S}| \overline{S_{ij}}. \tag{3}$$

Here, $\overline{\Delta} = 2(\Delta x \Delta y \Delta z)^{1/3}$ is the filter size, $\overline{S_{ij}} = \left(\partial \overline{u_i}/\partial x_j + \partial \overline{u_j}/\partial x_i\right)/2$ is the resolved strain-rate tensor and $|\overline{S}| = \left(2\overline{S_{ij}}\,\overline{S_{ij}}\right)^{1/2}$ is its magnitude. The coefficient C is determined using the dynamic model (Germano *et al.* 1991) with the Lagrangian averaging technique proposed by Meneveau *et al.* (1996), and extended to non-Cartesian geometries by Jordan (1999) and Armenio *et al.* (2000).

The governing differential equations (1) and (2) are discretized on a non-staggered grid using a curvilinear finite-volume code. The method of Rhie *et al.* (1983) is used to avoid pressure oscillations. Both convective and diffusive fluxes are approximated by second-order central differences. A second-order-accurate semi-implicit fractional-step procedure (Kim & Moin 1985) is used for the temporal discretization. The Crank-Nicolson scheme is used for the wall-normal diffusive terms, and the Adams-Bashforth scheme for all the other terms.

Fourier transforms are used to reduce the three-dimensional Poisson equation into a series of two-dimensional Helmholtz equations in wave-number space, which are solved iteratively using the Bi-Conjugate Gradient Stabilized method. The code is parallelized using the Message-Passing Interface and the domain-decomposition technique, and has been extensively tested for turbulent flows (Silva Lopes *et al.* 2006; Omidyeganeh *et al.* 2011).

The barchan model (Figure 1) was generated from the model used in the experiments of Palmer *et al.* (2011), which reflects a typical curvature of barchans in nature (Hersen *et al.* 2004). The aspect ratio of the current model falls in the range of laboratory and field measurements (Palmer *et al.* 2011). The barchan model has a length of $\lambda=3.62h$, width of $W=3.62h$, and height of $H=0.135h$. The ratio of the dune height to the channel height is equal to the ratio of the dune height to the boundary layer thickness in the experiment (Palmer *et al.* 2011). The simulation adopts an immersed boundary method based on the volume of fluid (VOF) technique (Scotti 2006) to model the barchan. On the bed, the no slip boundary condition is used. Periodic boundary conditions are used in the streamwise (x) and spanwise (z) directions. The flow is driven by a pressure gradient that maintains a constant streamwise flow-rate in time. The top surface is assumed to be rigid and free of shear stress: the vertical velocity is set to zero, as are the vertical derivatives of the streamwise and spanwise velocity components. The Reynolds number is $Re_\tau=25{,}160$ and is less than half of the experiments of Palmer *et al.* (2011; $Re_\infty=59{,}000$).

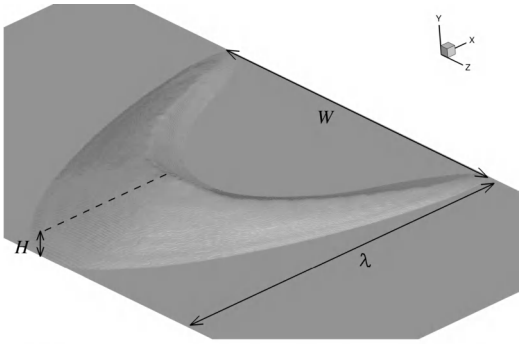

Figure 1. Geometry of the barchan dune model.

A series of simulations is conducted to study the effects of interdune spacing on the physics of flow (Table 1). A Cartesian mesh is generated; the grid distribution in the wall-normal direction is uniform up to the highest point of the dune, and then stretched by a hyperbolic tangent function. The grid in the spanwise direction is uniform, while in the streamwise direction a higher resolution is used over the lee side of the dunes, since the bed slope is significant in this zone and flow separates. For all cases mentioned in Table 1, the grid distribution is the same. We performed a grid refinement study for Case 1 with a focus on the resolution of the VOF model over the lee side of the dune as well as the convergence of statistics. Three simulations with 64 158 128, 128 158 256, and 160 281 512 grid points are examined and the finest simulation produces grid-converged results with resolution $\Delta x^+<28.86$, $\Delta y^+<0.83$, and $\Delta z^+<10.55$, where the plus sign in the superscript represents normalization with respect to the local bed-shear velocity u_τ and kinematic viscosity ν. First- and second-order statistics were within *5%* of each other for all resolutions. Only the results obtained with the finest grid resolution are shown in the following results. Note that the grid spacings above are comparable to those used in many Direct Numerical Simulations of the Navier-Stokes equations.

Table 1. Properties of the test cases. The interdune spacing is defined as the distance between the streamwise location of the horns of upstream dune and the upstream stoss side of the downstream dune.

Case No.	Spacing	$N_x \times N_y \times N_z$
1	0.00λ	160 281 512
2	0.34λ	192 281 512
3	0.68λ	224 281 512
4	1.02λ	256 281 512
5	2.38λ	384 281 512

The equations were integrated for $900H/U_\tau$ time units to remove transient effects. Then, statistics were accumulated over $1200H/U_\tau$ time units. To increase the sample size, averaging was also performed over the symmetric points in the spanwise direction. To verify the adequacy of the sample, we compared statistics obtained using only half of the sample with those obtained using the complete sample, and found that the mean velocities differed by less than *3%*, and the root-mean-square (rms) intensities by less than *7%*.

3. RESULTS

Mean streamwise velocity contours and streamlines on the centerline symmetry plane are shown for Case 5 in Figure 2. The flow separates at the crest and reattaches on the bed at $x_r/H \approx 5.6$. The reattachment length in the experiments is slightly smaller, which is explained by the faster flow over the crest in the simulations caused by the induced secondary flow (Figure 4). Decreasing the interdune spacing decreases the reattachment length not because of the speed of the approaching flow, but due to the bedward motion upstream of the dunes caused by the sheltering effect of the upstream dune.

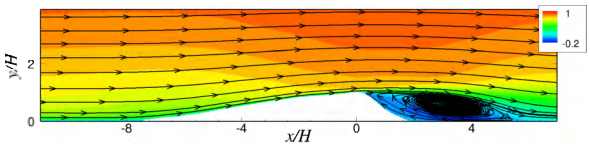

Figure 2. Contours of streamwise velocity normalized by the free stream velocity and streamlines on the centerline plane of Case 5.

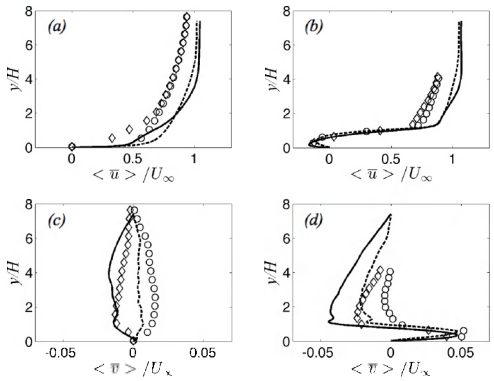

Figure 3. Normalized streamwise *(a,b)* and wall-normal *(c,d)* velocity profiles at *(a,c) x/H=-9.0*, and *(b,d) x/H=2.0*; — Case 5, - - - Case 1, O isolated dune, and ◊ zero interdune spacing in the experiment (Palmer *et al.* 2011).

Validation of our simulations is shown in Figure 3 for velocity profiles at two vertical lines upstream of the dune, *x/H=-9.0* and over the lee side of dune, *x/H=2.0*. The developed secondary flow across the channel in our simulations (Figure 4) drives high-momentum fluid into the centerline plane and causes the difference in the normalized bulk velocity profiles. Fluid moves faster on the centerline plane of the simulations, but the behavior of the velocity profiles is similar to the equivalent experiments (Palmer *et al.* 2011). The streamwise velocity profiles upstream of the dunes, in the zero-spacing cases, show a two-layer structure in which the wake with higher momentum overlies the internal boundary layer at the wall, and the two layers still interact. On the other hand, the isolated case shows a single layer similar to a boundary layer profile, and also similar to the largest interdune-spacing (Case 5), which indicates that there is a negligible wake effect at this distance (*60H* from the upstream crest). The two layer profiles have disappeared over the lee side (Figure 3*(b)*). The separation bubble is represented by negative streamwise velocities (Figure 2 and Figure 3*(b)*) and positive vertical velocity (Figure 3*(d)*) near the bed, *y/H<0.7*; here our simulations agree quantitatively with the experiments (Palmer *et al.* 2011).

Upstream of the dunes (Figure 3*(c)*), vertical velocity is positive for Case 5 and for the isolated dune in the experiments (Palmer *et al.* 2011) as the flow reacts to the windward slope. However, the upstream dune changes this feature; the approaching flow moves toward the bed (negative vertical velocities in Figure 3*(c)* for Case 1 and for the experiment with a zero spacing). This phenomenon influences the flow in the lee side of the downstream dune; the separation bubble shrinks due to the bedward bulk flow, and the reattachment length decreases.

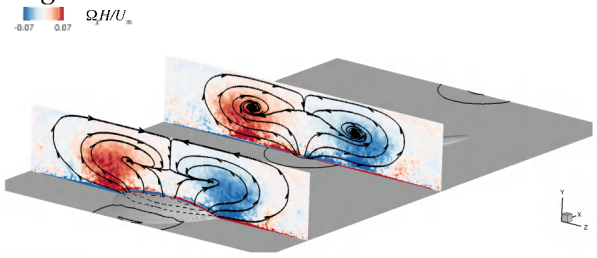

Figure 4. Contours of mean streamwise vorticity on two vertical planes across the channel at the crest and at the barchans toe for Case 3. Streamlines tangential to these planes show the secondary flow. Contour lines of the mean pressure are shown on the bed surface.

The profiles of the turbulence statistics show quantitative agreement with our simulations and with the experiments (Figure 5). Two peaks in the vertical profile of the turbulent kinetic energy (Figure 5*(b)*) for Case 1 represent two shear layers, with the overlying one being weaker. At the dune toe,

there is a near-bed peak representing the developing boundary layer on the stoss side for both simulations, while the second peak represents the wake region of the upstream dune for the zero-spacing case. Over the lee side, the outer-layer peak is still effective (at $y/H \approx 2.5$) while all cases show significant turbulent kinetic energy in the separated-shear layer. Reynolds shear stress is significant in the separated-shear layer as compared to the developing boundary layer.

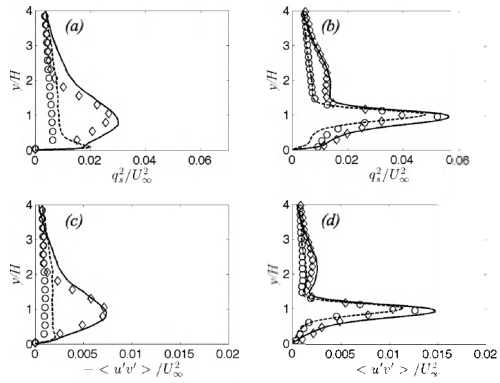

Figure 5. *(a,b)* Planar turbulent kinetic energy, $q_s^2 = (\langle u\,u\rangle + \langle v\,v\rangle)/2.0$, and *(c,d)* Reynolds shear stress at *(a,c) x/H=-9.0*, and *(b,d) x/H=2.0*; — Case 5, - - - Case 1, O isolated dune, and ◊ zero interdune spacing in the experiment (Palmer *et al.* 2011).

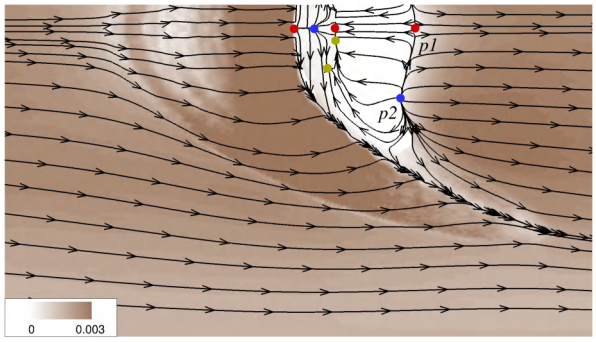

Figure 6. Contours of bed shear stress for Case 5. Streamlines represent the flow direction at the first grid point above the bed surface.

The bed shear-stress is strong over the stoss side of dunes close to the crest (Figure 6). At the toe, the flow diverges from the centerline plane, and the bed stress is decreased, but away from the centerline and along the horns the stress is large, as the flow rises up the stoss side. Figure 6 shows the size of the separation bubble that is not extended towards the horn. The separated flow at the crest reattaches to the bed and due to the three-dimensionality of the separation line, a nodal point of attachment is located away from the symmetry plane (point *p2* in Figure 6). The bed shear stress is larger downstream of this point where high-momentum fluid that separated at the crest reattaches, increases the pressure and the stress. Compared to the streamlines around the nodal point of reattachment, a saddle point of separation appears downstream of the dune on the symmetry plane (point *p1* in Figure 6) where the shear stress is small and the near-bed flow converges to the centerline plane from the sides. The separation bubble contains a large secondary flow, and a few small secondary flow regions over the lee side of the dune, which cause weak points of separation and attachment. These features close to the bed are often observed in the separation bubble of three-dimensional objects (Chapman *et al.* 1991). All other cases in our simulations present a similar trend; even the bed shear stress does not change significantly with the spacing. From a series of streamlines from the stoss side of the dune, we note that the separation bubble and the reattached flow converge to a single streamline along the horn and leave the dune from that side, consistent with 3D realizations of near-bed streamlines shown in Figure 7. The observation that barchan dunes loose sediment from the horns (Hersen *et al.* 2004 and Franklin *et al.* 2011), is explained by our results.

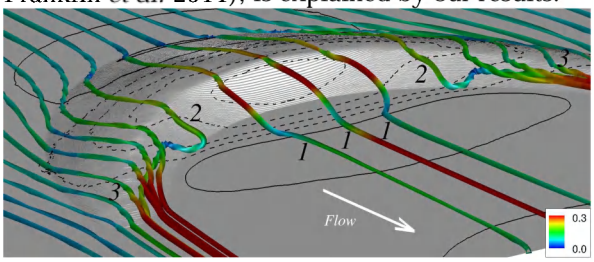

Figure 7. Streamlines close to the bed for the barchan dune of Case 3. Streamlines are colored with the magnitude of the velocity vector. Contour lines of mean pressure are shown on the bed surface; — $\langle \overline{p} \rangle = 0$. - - - $\langle \overline{p} \rangle = -0.005 \rho U_\infty^2$.

We show streamlines near the bed in Figure 7. Streamlines close to the centerline plane diverge and rise on the stoss side, then separate at the crest and move toward the bed while they are advected downstream (labeled by number 1). Away from the centerline plane, the streamlines diverge significantly toward the horns and separate at the crest,

but enter the separation bubble and meander in the recirculation region toward the horns while remaining near the bed (labeled by number 2). Streamlines far away from the centerline plane diverge toward the horns and never separate (labeled by number 3). Contours of the velocity magnitude show that streamlines moving toward the horns are accelerated.

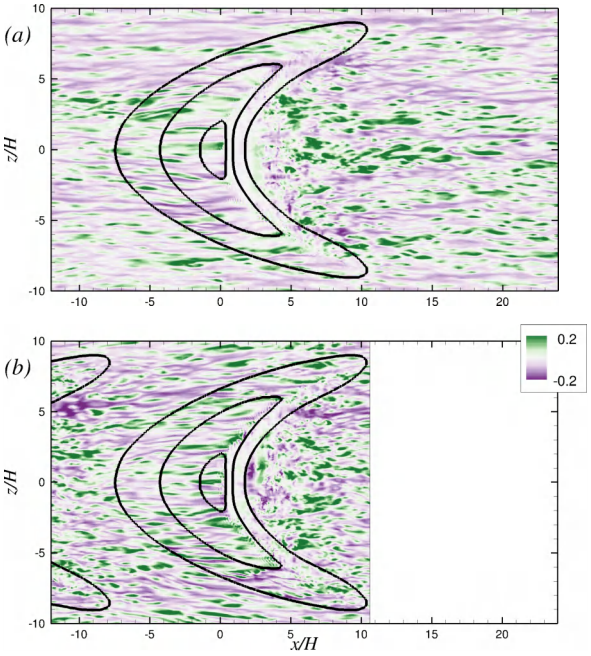

Figure 8. Contours of the streamwise fluctuating velocity on a plane parallel to the bed surface with a distance $0.025H$ for *(a)* Case 5, and *(b)* Case 1. The lines correspond to the bed levels at $y/H=0.03, 0.5\ 0.9$.

A realization of u' on a plane parallel and close to the bed is provided in Figure 8 for Case 5, with the largest interdune spacing, and Case 1, with the smallest interdune spacing. The flow approaching the dune in Case 5 has characteristics of a smooth open channel flow with alternating stripes of low- and high- momentum fluid. It seems that acceleration of flow over the stoss side of the dune elongates the streaks (Figure 8*(a)*). Franklin *et al.* (2011) observed streamwise stripes with regular spacing on the stoss side of their barchan dune. In the lee side of the dune, spanwise oriented structures are observed in between the horns. Around the reattachment region, the contours show a chaotic distribution of structures and after that, as the flow is advected downstream, the structures are reorganized and within a distance of an order of the dune length, the low- and high- speed streaks are reformed (Figure 8*(a)*). Case 1 (Figure 8*(b)*) presents different characteristics; the streaks are shorter and represent footprints of overlying turbulent events. The magnitude of fluctuations at the same distance from the bed is larger for Case 1 with smaller interdune spacing; hence this closely spaced arrangement of dunes enhances the wall turbulence and thus sediment transport in mobile bed barchans.

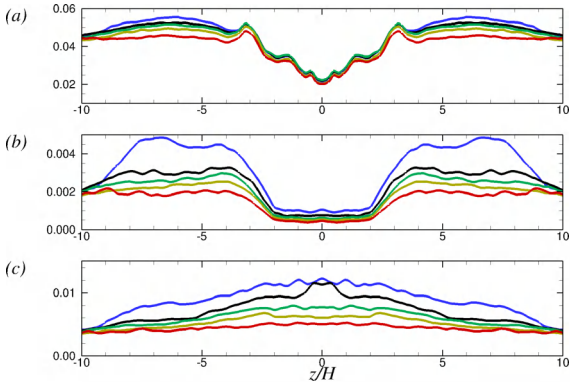

Figure 9. *(a)* Bed shear velocity, *(b)* wall-normal Reynolds normal stress, and **(c)** spanwise normal Reynolds stress at the centre of the stoss side $x/H=-5.0$ across the channel at a uniform distance from the bed. — Case 1, — Case 2, — Case 3, — Case 4, — Case 5.

At $x/H=-5.0$, in the middle of the stoss side, the mean bed-shear stress is not affected significantly by the interdune spacing (Figure 9*(a)* from $-3.5<z/H<3.5$), but the turbulent activities are significantly altered; *e.g.*, the spanwise normal Reynolds stress (Figure 9*(c)*) has a peak on the centerline of the dune and is larger for a smaller interdune spacing. Around the edges of the dune surface, at $z/H\approx\pm3.5$, the wall-normal stress (Figure 9*(b)*) is boosted and is larger for closely spaced dunes.

Instantaneous flow structures are shown by the Q criterion, where

$$Q=-\frac{1}{2}\frac{\partial\bar{u}_j}{\partial x_i}\frac{\partial\bar{u}_i}{\partial x_j} \qquad (4)$$

for Cases 1 (Figure 10) and 5 (Figure 11). A population of coherent structures over the stoss side is evident in Case 1. Away from the dunes, typical wall turbulence structures are observed, but coherent eddies generated in the separated-shear layer due to Kelvin-Helmholtz instability are dominant. Separated vortices in Case 5 are advected away

from the centerline plane by the secondary flow (Figure 4) and dissipate before reaching the downstream dune. In Case 1, the production of these structures is more frequent, and they do not diverge from the centerline plane since the spacing between the dunes is small. Hence, we observe more structures in Case 1 between the horns.

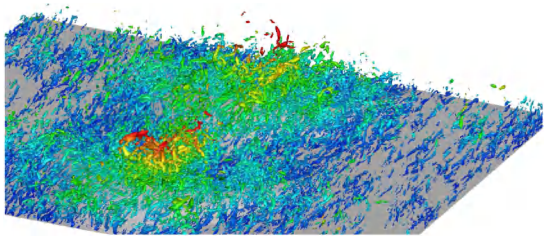

Figure 10. Isosurfaces of the second invariant of the velocity gradient tensor, $QH^2/U_r^2=0.7$, colored by distance from the bed for Case 1 (refer to Figure 11 for the scales).

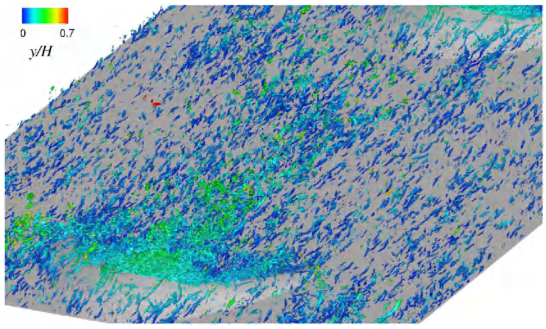

Figure 11. Isosurfaces of the second invariant of the velocity gradient tensor, $QH^2/U_r^2=0.7$, colored by distance from the bed for Case 5.

4. CONCLUSIONS

Flow over barchan dunes has some characteristics in common with that over transverse dunes (deceleration and acceleration of flow over the stoss side, separated flow and formation of a shear layer at the crest, reattachment of flow on the bed and development of internal boundary layer), but the complex three-dimensional shape of barchans introduces mean secondary flow across the channel and alters turbulence over the stoss side. The current simulations are validated against experiments (Palmer *et al.* 2011) and provide a comprehensive three-dimensional realization of mean flow characteristics and instantaneous flow structures.

Barchan dunes induce two counter-rotating streamwise vortices, each along one of the horns. These vortices direct high-momentum fluid toward the centerline symmetry plane and low-momentum fluid near the bed away from the centerline. In our configuration with barchans aligned in the spanwise direction, and with the periodic boundary condition we use, the streamwise vortices become stable.

The three-dimensional flow visualization explains some features of sediment transport near the bed reported in the literature; the flow decelerates at the toe of the dune and moves toward the closest horn, hence bed shear stress increases on the sides of the barchan while it decreases on the centerline plane. Separation of the flow at the horns is intermittent; 3D streamlines show that the flow at the crest may enter the separation bubble and meander toward the horns and leave the dune while accelerating. We note that flow in the separation bubble is likely capable of transporting high concentrations of sediment and exiting the dune from the horns, which explains many observations in nature and laboratory measurements that barchans loose sediment downstream via their horns.

The interdune spacing quantitatively alters the mean flow; the secondary flow is stronger at smaller spacings, and the sheltering effect of the upstream dune is observed in the turbulence characteristics; coherent high- and low-speed streaks are shorter and the spanwise Reynolds normal stress is significantly higher where the interaction between the wake region and the internal boundary layer is strong.

5. ACKNOWLEDGMENTS

The authors are grateful to the High Performance Computing Virtual Laboratory (HPCVL), Queen's University site, for computational support. MO acknowledges the partial support of NSERC under the Alexander Graham Bell Canada NSERC Scholarship Program. UP also acknowledges the support of the Canada Research Chairs Program and of the Natural Sciences and Engineering Research Council (NSERC) under the Discovery Grant program.

6. REFERENCES

Allen, J. 1968. Current ripples: their relation to patterns of water and sediment motion. North-Holland Pub. Co.

Armenio, V. & Piomelli, U. 2000. A Lagrangian Mixed Subgrid-Scale Model in Generalized Coordinates. Flow. Turb. Combust., 65, 51–81.

Baddock, M. C., Livingstone, I. & Wiggs, G. F. S. 2007. The geomorphological significance of airflow patterns in transverse dune interdunes. Geomorphology, 87, 322–336.

Bagnold, R. A. 1941. The Physics of Blown Sand and Desert Dunes. Methuen, London.

Breed, C. S., Grolier, M. J. & McCauley, J. F. 1979. Morphology and distribution of common 'sand' dunes on mars: Comparison with the earth. J. Geophys. Res., 84, 8183–8204.

Chapman, G. T. & Yates, L. A. 1991. Topology of flow separation on three-dimensional bodies, Appl. Mech. Rev., 44(7), 329–345.

Charru, F. & Franklin, E. M. 2012. Subaqueous barchan dunes in turbulent shear flow. part 2. fluid flow. J. Fluid Mech., 694, 131–154.

Fernandez, R., Best, J. and Lopez, F., 2006 Mean flow, turbulence structure and bedform superimposition across the ripple-dune transition, Wat. Resources Res., 42, W05406, doi:10.1029/2005WR004330.

Frank, A. & Kocurek, G. 1996. Toward a model for airflow on the lee side of aeolian dunes. Sedimentology, 43, 451–458.

Franklin, E. M. & Charru, F. 2011. Subaqueous barchan dunes in turbulent shear flow. part 1. dune motion. J. Fluid Mech., 675, 199–222.

Germano, M., Piomelli, U., Moin, P. & Cabot, W. H. 1991. A dynamic subgrid-scale eddy viscosity model, Phys. Fluids A, 3, 1760–1765.

Hermann, H. J., Andrade Jr., J. S., Schatz, V., Sauermann, G. & Parteli, E. J. R. 2005. Calculation of the separation streamlines of barchans and transverse dunes. Physica A, 357, 44–49, doi:10.1016/j.physa.2005.05.057.

Hersen, P., Andersen, K. H., Elbelrhiti, H., Andreotti, B., Claudin, P. & Douady, S. 2004. Corridors of barchan dunes: Stability and size selection. Phys. Rev. E, 69 (011304), 1–12.

Hesp, P. A. & Hastings, K. 1998. Width, height and slope relationships and aerodynamic maintenance of barchans. Geomorphology, 22, 193–204.

Jordan, S. A. 1999. A large-eddy simulation methodology in generalized curvilinear coordinates, J. Comput. Phys., 148(2), 322–340.

Kim, J. & Moin, P. 1985. Application of a fractional step method to incompressible Navier-Stokes equations. J. Comput. Phys., 59, 308–323.

Kroy, K., Fischer, S. & Obermayer, B. 2005. The shape of barchan dunes. J. Phys. Condens. Matter, 17, S1229–S1235.

Lancaster, N. 1985. Variations in wind velocity and sand transport rates on the wind-ward flanks of desert sand dunes. Sedimentology, 32, 581–593.

Lancaster, N. 1995. Geomorphology of desert dunes, Routledge, New York.

Lancaster, N., Nickling, W. G., McKenna Neuman, C. & Wyatt, V. E. 1996. Sediment flux and airflow on the stoss slope of a barchan dune. Geomorphology, 17, 55–62.

Lettau, K. & Lettau, H. H. 1969. Bulk transport of sand by the barchans of la pampa la hoja in southern Peru. Zeitschrift fūr Geomorphologie, 13, 182–195.

McCullogh, D. S. & Janda, R. J. 1964. Subaqueous river channel barchan dunes. J. Sed. Petrol., 34, 694.

McKenna Neuman, C., Lancaster, N. & Nickling, W. G. 2000. The effect of unsteady winds on sediment transport on the stoss slope of a transverse dune, silver peak, NY, USA. Sedimentology, 47, 211–226.

Meneveau, C., Lund, T. S. & Cabot, W. H. 1996. A Lagrangian dynamic subgrid-scale model of turbulence. J. Fluid Mech., 319, 353–385.

Omidyeganeh, M. & Piomelli, U. 2011. Large-eddy simulation of two-dimensional dunes in a steady, unidirectional flow. J. Turbul., 12 (42), 1–31.

Palmer, J. A., , Mejia-Alvarez, R., Best, J. L. & Christensen, K. T. 2011. Particle-image velocimetry measurements of flow over interacting barchan dunes. Exp. Fluids, pp. 1–21.

Parsons, D. R., Wiggs, G. F. S., Walker, I. J., Ferguson, R. I. & Garvey, B. G. 2004. Numerical modelling of airflow over an idealised transverse dune. Env. Mod. Soft., 19, 153–162, doi:10.1016/S1364-8152(03)00117-8.

Rhie, C. M. & Chow, W. L. 1983. Numerical study of the turbulent flow past an airfoil with trailing edge separation. AIAA J., 21, 1525–1532.

Scotti, A. 2006. Direct numerical simulation of turbulent channel flows with boundary roughened with virtual sandpaper. Phys. Fluids, 18, 031,701.

Silva Lopes, A., Piomelli, U. & Palma, J. M. L. M. 2006. Large-eddy simulation of the flow in an S-duct. J. Turbul., 7 (11), 1–24.

Takahashi, S., Du, M., Wu, P., Maki, T. & Kawashima, S. 1998. Three dimensional numerical simulation of the flow over complex terrain with windbreak hedge. Env. Mod. Soft., 13, 257–265.

Walker, I. J. & Nickling, W. G. 2003. Simulation and measurement of surface shear stress over isolated and closely spaced transverse dunes in a wind tunnel. Earth Surf. Proc. Landf., 28, 1111–1124.

Wiggs, G. F. S., Livingstone, I. & Warren, A. 1996. The role of streamline curvature in sand dune dynamics: evidence from field and wind tunnel measurements. Geomorphology, 17, 29–46.

Wippermann, F. K. & Gross, G. 1986. The wind-induced shaping and migration of an isolated dune: a numerical experiment. Bound.-Lay. Meteorol., 36, 319–334.